Perspective on the refractive-index gas metrology data landscape

Rourke, Patrick M. C.

Publisher's version / Version de l'éditeur:
https://doi.org/10.1063/5.0055412
Journal of Physical and Chemical Reference Data, 50, 3, pp. 1-14, 2021-09-13

Perspective on the refractive-index gas thermometry data landscape

Patrick M. C. Rourke[a)]
National Research Council Canada, Ottawa K1A 0R6, Canada

(Dated: 26 March 2021)

The redefinition of the kelvin has increased focus on primary thermometry techniques that use the newly-fixed value of the Boltzmann constant to directly realize thermodynamic temperature. One such technique that has advanced considerably in recent years is refractive-index gas thermometry (RIGT). This also includes a range of applications outside of temperature metrology, such as primary pressure standards to replace mercury manometers and measurements of the thermophysical properties of gases. Here the current data situation in the field is reviewed, encompassing the latest developments and remaining challenges, in order to suggest possible approaches for reducing dominant RIGT uncertainties and improving RIGT applications.

New analyses of the second density virial coefficient B_ρ and the third dielectric virial coefficient C_ϵ of helium, neon and argon are performed on existing experimental literature data. A need is identified for more accurate reference-quality data sets to be measured or calculated in several areas, with robust uncertainty budgets, to support future RIGT advancements: the bulk modulus of copper; thermodynamic inaccuracy of the International Temperature Scale of 1990; molar electric polarizability A_ϵ of neon and argon; diamagnetic susceptibility χ_0 of argon; second density virial coefficient B_ρ of neon and argon; third dielectric virial coefficient C_ϵ of helium, neon and argon; and third refractivity virial coefficient C_R of neon.

Keywords: Refractive-index gas thermometry; RIGT; pressure; polarizability; compressibility; virial coefficients

1. Introduction

1.1. Redefinition of the kelvin

The revision of the International System of Units (SI) that went into effect on 20 May 2019 fixed the numerical values of four fundamental constants—the Boltzmann constant k_B, the Avogadro constant N_A, the Planck constant h and the elementary charge e—and used these in new definitions for base units of the SI. The whole of the SI now uses the fundamental rules of nature to create the rules of measurement.[1]

Previously, the SI unit of thermodynamic temperature, the kelvin, was based on the temperature of the triple point of water. However, the physical meaning of thermodynamic temperature is the average thermal energy per degree of freedom in a given system. The new definition of the kelvin directly embodies this understanding, with the Boltzmann constant simply acting as the conversion factor between the unit of energy and the (more convenient) unit of temperature.[2]

The new definition of the kelvin has put a spotlight on primary thermometers that can leverage the fixed value of the fundamental constant k_B to access thermodynamic temperature over a wide temperature range, now unshackled from the triple point of water.[1] The *Mise en pratique* for the definition of the kelvin in the SI (*MeP*-K) describes several primary methods for realizing this unit in practice.[3] The goal of the present work is to summarize key aspects of the data landscape related to one of these methods: refractive-index gas thermometry (RIGT).

A review of RIGT already exists[4] to support the purpose of the *MeP*-K,[3] but significant experimental and theoretical advancements have blossomed since its publication. The present article encompasses the latest RIGT developments and remaining challenges, particularly as viewed through a reference data lens, including application to other metrology areas beyond the realization of the kelvin.

1.2. What is refractive-index gas thermometry?

The core idea of RIGT is simple: denser gas refracts light more strongly than less dense gas. Combining this idea with the ideal gas law gives an approximate working equation:

$$n^2 - 1 \approx 3\left(A_\epsilon + A_\mu\right)\frac{p}{N_\mathrm{A} k_\mathrm{B} T}, \tag{1}$$

where properties of the gas are the refractive index n, the thermodynamic temperature T, the pressure p, the zero-density limit of the molar electric polarizability A_ϵ, and the zero-density limit of the molar magnetic susceptibility A_μ.[4]

An experimental measurement of n can be used to determine the value of one of the quantities on the right hand side of Eq. 1, provided the values of the others are independently known. If A_ϵ, A_μ and p are known, the refractive index measurement becomes a T measurement, often used alongside traditional resistance thermometry to measure how well temperatures T_{90} on the International Temperature Scale of 1990 (ITS-90) approximate thermodynamic temperature.[5–10] If A_ϵ, A_μ and T are known, the refractive index measurement becomes a p measurement, providing a primary thermodynamic pres-

[a)] patrick.rourke@nrc-cnrc.gc.ca

sure standard that may be used as an alternative to mercury manometers.[11–15] And if A_μ, T and p are known, the refractive index measurement becomes an A_ϵ measurement, revealing a fundamental property of the gas species.[11,16,17] RIGT techniques have also been used to characterize the dimensions of a variety of small and large containers,[16,18–22] to measure humidity in air and natural gas,[23–25] and, prior to the redefinition of the kelvin, to measure the Boltzmann constant k_B.[11,26] Although only the first application is "thermometry," in the present work the acronym RIGT is used to cover all of the above uses of the technique.

In practice, the idealized working equation 1 must be expanded to include higher-order corrections due to multi-particle interactions that occur in real gases:

$$\frac{n^2-1}{n^2+2} = \sum_{i=1}^{\infty} A_i \left(\frac{p}{N_\mathrm{A} k_\mathrm{B} T}\right)^i, \tag{2}$$

in which

$$A_1 = A_\epsilon + A_\mu, \tag{3}$$

$$A_2 \approx B_\epsilon - A_\epsilon B_\rho, \tag{4}$$

$$A_3 \approx C_\epsilon - 2B_\epsilon B_\rho + 2A_\epsilon B_\rho^2 - A_\epsilon C_\rho, \tag{5}$$

and so on. The higher dielectric virial coefficients B_ϵ, C_ϵ, etc. and higher density virial coefficients B_ρ, C_ρ, etc. respectively embody the higher-order dependencies of polarizability and of pressure on the molar density of the gas. The first term of Eq. 2 corresponds to Eq. 1, while the other terms become progressively more important at higher gas densities (larger p and/or smaller T).[4]

Equations 2–5 above replace Eqs. 13–16 from Ref. 4 because those of the present work are based on a more accurate simplification of Eq. 12 from Ref. 4 compared to the simplification written in Eq. 8 from Ref. 4. Even higher accuracy may be obtained by directly using Eqs. 12 and 4 from Ref. 4 without simplification.[5,7]

Modern RIGT exploits the sensitivity of frequency-domain measurements in order to perform precise experimental determinations of the refractive index. This naturally divides RIGT implementations into two groups: those measuring n at microwave frequencies (low GHz range)[5–9,11,16,18–25] and those measuring n at optical frequencies (hundreds of THz).[10,12–15,17,26–30]

Microwave RIGT obtains n from measurements of the electromagnetic resonance frequencies supported by conducting cavities, usually quasi-spherical in shape[5,7–9,11,16,18,20,23–25] but sometimes cylindrical,[6,19,21,22] and often constructed of copper[5–9,16,18,20,22] but sometimes steel[11,21,23–25] or more exotic materials.[19] Microwave RIGT shares many similarities with its sibling primary gas thermometry methods dielectric-constant gas thermometry (DCGT)[3,31] and acoustic gas thermometry (AGT).[3,32]

Optical RIGT obtains n using interferometric measurements of laser light passing through gas cells usually constructed of low-expansion glass[10,12,14,15,17,26–28]

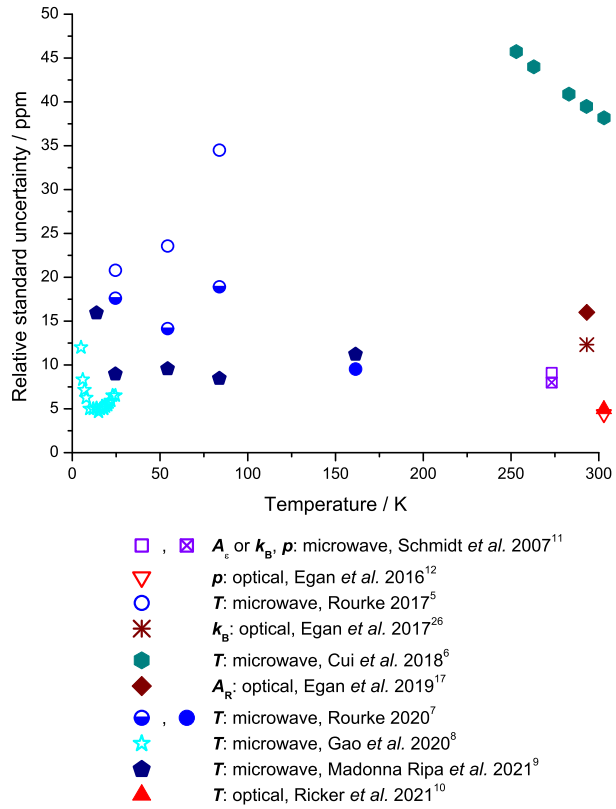

FIG. 1. Relative standard uncertainties of different experimental RIGT implementations.

but sometimes other materials such as Invar.[29,30] While the electromagnetic frequencies used in microwave RIGT are low enough that static versions of A_ϵ, A_μ and the higher dielectric virial coefficients are acceptable, taking account of the frequency dependence is important for optical RIGT.[4,13]

Relative uncertainties of a selection of recent RIGT implementations are shown in Fig. 1. All uncertainties in the present work have been converted to standard uncertainties ($k = 1$), not expanded uncertainties. To facilitate comparison across a variety of RIGT applications, relative uncertainties are expressed in abbreviated form as parts per million ("ppm") or parts per hundred ("%"): for example, a 1 ppm $= 1 \times 10^{-6}$ relative uncertainty would correspond to 1 µK K^{-1} for a RIGT T measurement or 1 µPa Pa^{-1} for a RIGT p measurement.

1.3. Outline

Section 2 summarizes the main categories of RIGT uncertainty components and recent RIGT development progress that has allowed the technique to evolve beyond earlier limitations. Drawing on these recent advancements, the latest data and approaches for handling the three dominant sources of RIGT uncertainties are described, along with what data need to be measured or

calculated better to further improve RIGT performance: physical properties of the solid materials used in the construction of refractive-index gas thermometers (Sec. 3); gas pressure, temperature and impurities (Sec. 4); and thermophysical properties of the RIGT working gases (Sec. 5). Lastly, Sec. 6 presents some concluding remarks.

2. RIGT uncertainties: past and present

2.1. Main sources of uncertainty

The most obvious way to implement RIGT is to measure the refractive index n at a single (p, T) thermodynamic state and use this to evaluate Eq. 2 at that state only.[4] This absolute single-state approach was the dominant RIGT method at the time of publication of Ref. 4 and provides a good baseline for the discussion of RIGT uncertainties.

Comparing the microwave or optical measurements made at (p, T) with those made using the same apparatus in vacuum, where $n \equiv 1$, allows many systematic effects to be cancelled out. But pressure-induced compression and distortions of the solid parts of the apparatus between vacuum and p can have a big influence on the apparent value of n. Therefore the ability to correct for these effects and other physical properties of the apparatus forms the first major category of RIGT uncertainty component (Sec. 3).

Next, since all but one of the quantities on the right hand side of Eq. 2 must be independently known, and all terms include both p and T, non-RIGT measurements of the thermodynamic pressure and/or thermodynamic temperature of the working gas give rise to the second major category of RIGT uncertainty component (Sec. 4). That is, an absolute single-state RIGT primary temperature realization cannot beat the uncertainty of its supporting gas pressure measurement, and an absolute single-state RIGT primary pressure realization cannot beat the uncertainty of its supporting gas temperature measurement. Knowledge of the working gas composition is also important, because A_ϵ appears in all terms of Eq. 2 and different gases can have vastly different polarizabilities.

Finally, all of the virial coefficients within the terms of Eq. 2 that contribute significantly at (p, T) are in play, so the accuracy of these gas thermophysical properties comprises the third major category of RIGT uncertainty component (Sec. 5). A_ϵ is particularly crucial, because it is present in Eq. 2 at first order, but other virial coefficients can be important too. Choosing (p, T) states with higher gas densities usually improves the signal-to-noise ratio of the experimental n measurements, but with a trade-off that the more uncertain higher-order terms of Eq. 2 contribute more strongly. Insufficient knowledge of the higher virial coefficients of all other gases effectively limits absolute single-state RIGT to using helium as the working gas, but helium only weakly refracts light, so helium-based RIGT is very sensitive to uncertainties from the other two categories: apparatus distortions and gas impurities.

2.2. Recent advancements

Several improvements over the absolute single-state method that were anticipated in Ref. 4 have now been realized in practice.

The effects of pressure on the solid parts of a RIGT apparatus are now measured *in situ*,[7,9,10,12] rather than relying exclusively on generic material properties published in the literature. This need only be done once for a given apparatus, and reduces RIGT uncertainties from the first category. The measurements are done at known p and T, and extrapolated to other temperatures using a method originally developed for DCGT.[33] This transforms the technique into an indirect form of relative RIGT, because subsequent measurements rely on the distortion characterization performed at a particular known thermodynamic state.

Relative single-state RIGT has now also been directly implemented.[8] Measurements are performed on isobars rather than isotherms, and analyzed in ratio with an isobar point taken at a known T_{ref}. This leads to several key advantages: first-order p contributions to Eq. 2 cancel out, alleviating a major RIGT weakness from the second uncertainty category; the absolute compressibility of the apparatus no longer matters, only the relative temperature-dependence between T_{ref} and the other temperatures on the isobar, reducing uncertainty contributions from the first category; and the measurements can be performed very quickly. This method was successfully used below 25 K, where physical properties of the apparatus are largely temperature-independent.[8] However, it has its own limitations in that it is dependent on an external primary realization of T_{ref}, and has limited prospects for use at higher temperatures.[8]

Another advancement is the implementation of the "hybrid" data analysis method that was proposed in Ref. 4: RIGT measurements are made at many pressures on an isotherm, each analyzed separately as in the single-state method using best guesses for the higher virial coefficients, and then extrapolated to $p = 0$ using a low-order fit function.[7,9] This greatly weakens the influence of the higher virials, reducing RIGT uncertainties from the third category. Moreover, this also opens the door to using non-helium working gases, which in turn reduce RIGT uncertainties from the first and second categories. The downside is that this method is potentially much slower than the single-state method, which does not require measurements on isotherms.

A further strategy involves repeating measurements at the same (p, T) states using two different working gases.[4,17] Since the two gases have differing refractivity, but in both cases the pressure-induced compression and distortions of the apparatus are the same, the mea-

surements can be combined in ratio in order to minimize uncertainties from the first category. This approach doubles the measuring time and has other caveats,[4] but has now been successfully implemented in practice.[9,30] Experimental realization of this two-gas strategy was found to be helpful for optical RIGT p measurements using helium and nitrogen,[30] but less so for microwave RIGT T measurements using helium and neon.[9]

New, more accurate *ab initio* calculations of the thermophysical properties of helium and other gases[34–41] have also been performed since the publication of Ref. 4, reducing RIGT uncertainty contributions from the third category.

Other recent improvements have been developed specifically for optical RIGT. A technique that rapidly oscillates the gas between pressure p and vacuum reduces the effects of fluctuations and drift of cavity length, gas leaks, gas permeation and out-gassing.[27,28] This allows the apparatus to be constructed from non-glass materials such as Invar, that have lower compressibility, better temperature stability and better temperature uniformity than glass.[29] And the addition of a Littrow external cavity diode laser with a widely tunable frequency broadens the range of (p, T) states that may be continuously accessed without stopping to change the resonant order of the cavity.[15]

3. Compressibility and other physical properties of the experimental apparatus

3.1. Microwave RIGT: copper compressibility

All modern microwave RIGT realizations that extend significantly below room temperature have used hollow resonating cavities constructed of copper,[5–9] and therefore knowledge of how these compress under pressure forms a key component of the RIGT data landscape.[4] The effective isothermal compressibility of a copper cavity shell $\kappa_{\mathrm{T,eff}}$ is nearly temperature-independent below 25 K and therefore mostly cancels out of relative RIGT measurements performed below this temperature using $T_{\mathrm{ref}} = 25\,\mathrm{K}$.[8] But other microwave RIGT implementations suffer a contribution from the uncertainty in $\kappa_{\mathrm{T,eff}}$ to the absolute uncertainty in T that scales as T^2,[5,9] often dominating uncertainty budgets when helium is used as the working gas.

The most accurate assessment of $\kappa_{\mathrm{T,eff}}$ can be obtained by measuring the compression of the resonating cavity directly using RIGT techniques at a reference temperature T_{ref} (usually TPW),[7,9] and then extrapolating this to other temperatures T.[33] When RIGT data that was originally analyzed[5] using κ_{T} values solely drawn from the literature[42] (open circles in Fig. 1) was re-analyzed using the *in situ* extrapolated $\kappa_{\mathrm{T,eff}}$, uncertainties decreased significantly[7] (half-filled circles in Fig. 1).

The extrapolation is based on the theory of Grüneisen[43] and operates on the adiabatic compressibility κ_{S}, which is the inverse of the adiabatic bulk modulus B_{S}:[7,9,33]

$$\kappa_{\mathrm{S,extrap}}(T) = \kappa_{\mathrm{S,meas}}(T_{\mathrm{ref}}) \left[\int_{T_{\mathrm{ref}}}^{T} \alpha_{\mathrm{L}}(T^*) \mathrm{d}T^* \right]^{3\delta} \quad (6)$$

where α_{L} is the linear thermal expansion coefficient (the volumetric thermal expansion coefficient is $\alpha_{\mathrm{V}} \approx 3\alpha_{\mathrm{L}}$), and the Anderson-Grüneisen parameter δ is[33]

$$\delta = \frac{\partial \left(\ln \kappa_{\mathrm{S}} \right) / \partial T}{3\alpha_{\mathrm{L}}}. \quad (7)$$

Conversion between κ_{S} and κ_{T} is straightforward:[5,7,9,33]

$$\kappa_{\mathrm{T}} = \kappa_{\mathrm{S}} \left[1 + \gamma T \left(3\alpha_{\mathrm{L}} \right) \right], \quad (8)$$

where

$$\gamma = \frac{3\alpha_{\mathrm{L}}}{\kappa_{\mathrm{S}} c_{\mathrm{p}} \rho_{\mathrm{solid}}} \quad (9)$$

is the Grüneisen parameter, c_{p} is the constant-pressure specific heat capacity and ρ_{solid} is the mass density of solid copper.

According to Grüneisen, δ should be temperature-independent, so RIGT and DCGT workers typically take the value of δ from external resonant ultrasound spectroscopy or literature measurements of B_{S} over a restricted temperature range near room temperature and use this single δ value to extrapolate the *in-situ* measured compressibility to all temperatures of interest.[7,9,33] But Grüneisen's theory relies on many simplifying assumptions.[33] Figure 2 shows that when δ is calculated from experimental B_{S} measurements of monocrystalline[44] and polycrystalline[45] oxygen-free high-conductivity (OFHC) copper spanning a wide temperature range, temperature dependence develops at lower temperatures. A reference data set[42] that combines the monocrystalline[44] and polycrystalline[45] measurements has large uncertainties and different temperature dependence than either source data set. Recent resonant ultrasound spectroscopy B_{S} measurements of polycrystalline electrolytic-tough-pitch (ETP) copper[9] agree with the OFHC copper data[44,45] in their region of overlap.

The same historical OFHC copper literature B_{S} data sets[44,45] can be used to test the internal consistency of the Eq. 6–7 extrapolation scheme by converting the highest-temperature measured B_{S} to $\kappa_{\mathrm{S,meas}}$, extrapolating it to lower temperatures as $\kappa_{\mathrm{S,extrap}}$ using a single δ value taken from the region in which δ is temperature independent, and then comparing to $\kappa_{\mathrm{S,meas}}$ converted from the directly-measured B_{S} values at those temperatures. Figure 3 shows that $\kappa_{\mathrm{S,extrap}}$ begins to deviate from $\kappa_{\mathrm{S,meas}}$ at around 100–200 K. (The internal extrapolation consistency is much poorer if B_{S} from Ref. 42 is used, since its δ exhibits stronger temperature dependence across the whole temperature range.)

Both $\partial \left(\ln \kappa_{\mathrm{S}} \right) / \partial T$ and α_{L} decrease with decreasing temperature, causing the ratio in Eq. 7 to become increasingly unreliable and sensitive to small, uncontrolled

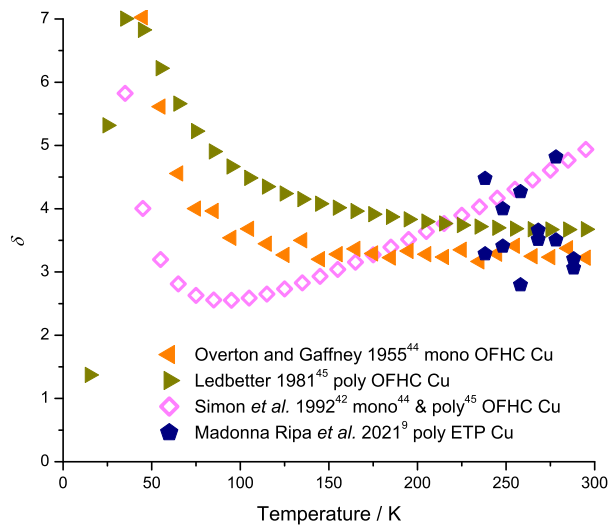

FIG. 2. Experimentally-measured temperature dependence of the Anderson-Grüneisen parameter δ for copper.

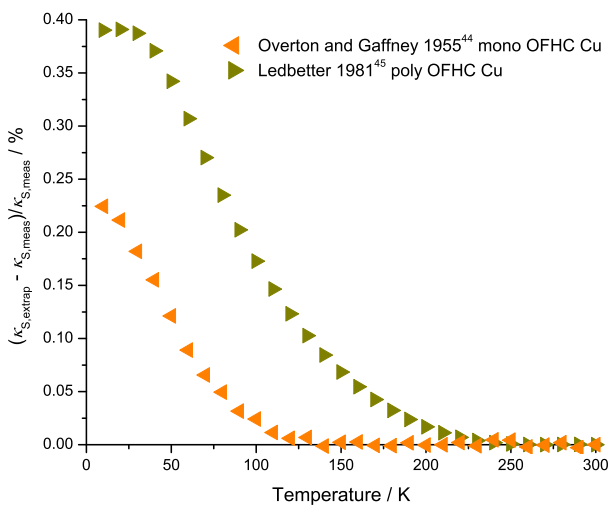

FIG. 3. Internal consistency tests of copper compressibility extrapolation.

experimental effects. This probably causes the extreme behaviour seen at the lowest temperatures in Fig. 2. However, the temperature dependence of δ in Fig. 2 and deviation of $\kappa_{\mathrm{S,extrap}}$ from $\kappa_{\mathrm{S,meas}}$ in Fig. 3 both begin smoothly at much higher temperatures, where $\partial\left(\ln\kappa_{\mathrm{S}}\right)/\partial T$ and α_{L} are not very different from their room-temperature values: $\partial\left(\ln\kappa_{\mathrm{S}}\right)/\partial T$ falls to half of its room-temperature value around 60 K and half again around 30–40 K;[44,45] and α_{L} falls to half of its room-temperature value around 80 K and half again around 50 K.[20,42] Thus, the inconsistency of the κ_{S} extrapolation might be due to a breakdown of the assumptions underlying the theory of Grüneisen.

The implications for RIGT can be seen, for example, in the experimental results described in Ref. 7 using helium as the working gas. Although this resonator was

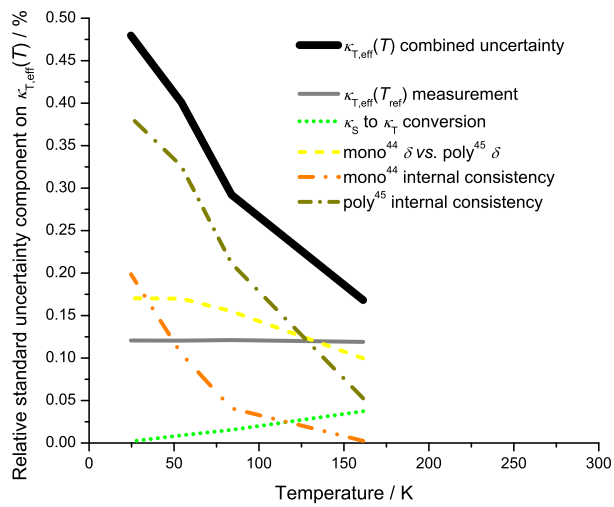

FIG. 4. Relative uncertainty components on extrapolated $\kappa_{\mathrm{T,eff}}$ values.[7]

constructed of two pieces of machined polycrystalline OFHC copper, the compressibility measured *in situ* at TPW using microwaves was much closer to that of the historical monocrystalline[44] rather than polycrystalline[45] data. Lacking any further information, the compressibility extrapolation was performed with δ values calculated from high-temperature portions of both literature data sets,[44,45] including uncertainty contributions from both.[7] Figure 4 shows that the uncertainty of the extrapolated $\kappa_{\mathrm{T,eff}}$ used in the RIGT analysis[7] is dominated below about 100 K by the inconsistency of extrapolation revealed by internal tests of the historical polycrystalline data[45] (Fig. 3).

The sensitivity of the thermodynamic temperature T to the compressibility of the resonator shell is itself temperature dependent, such that the uncertainty components on $\kappa_{\mathrm{T,eff}}$ contribute less strongly to the uncertainty budget of T at lower temperatures. However, Fig. 5 shows that the inconsistency of the compressibility extrapolation based on Grüneisen's constant-δ theory still contributes considerable uncertainty to T between 50 K and 100 K.

In Ref. 9, the microwave resonator was instead constructed of polycrystalline ETP copper, and the δ value used for compressibility extrapolation came from new bulk modulus measurements of samples of the same material (pentagon symbols in Fig. 2). In this case, the "mono[44] δ *vs.* poly[45] δ" curve seen in Figs. 4 and 5 is replaced with one propagated from the uncertainty in the new measured δ value. The historical OFHC Cu data[44,45] were no longer needed, but the ETP Cu data[9] are confined to a restricted temperature range that is too high to give any information on possible breakdown of Grüneisen's assumptions, temperature-dependence of δ or internal inconsistency of the compressibility extrapolation procedure.

In order to resolve whether the deviations seen in

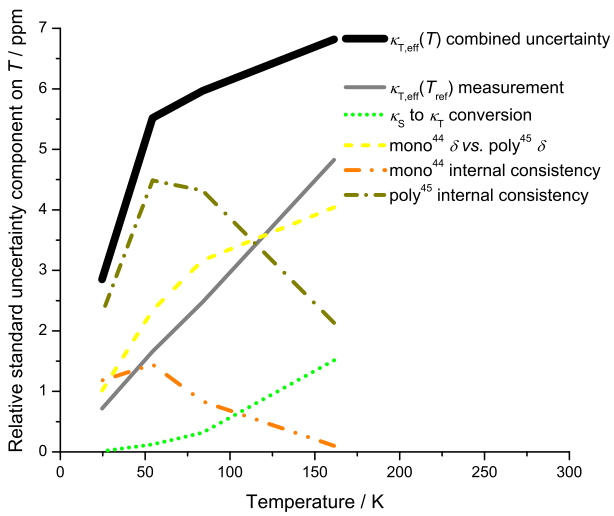

FIG. 5. Relative uncertainty components on T of extrapolated $\kappa_{\mathrm{T,eff}}$ values.[7]

Figs. 2 and 3 truly represent a breakdown of the compressibility extrapolation method[33] based on the theory of Grüneisen[43] or simply arise from experimental non-idealities of the historical reference data sets,[44,45] new highly-accurate experimental reference measurements of the bulk modulus of copper between 4 K and 300 K are needed. If the deviations are not caused by experimental effects, it would be further useful to know whether they differ significantly between monocrystalline and polycrystalline copper (as suggested by Figs. 2–5), between OFHC and ETP copper, and from sample to sample. Ultimately, such reference data should lead to lower and better-estimated RIGT uncertainties.

3.2. Microwave RIGT: other properties of copper

The reference data situation for other relevant properties of copper is already satisfactory for RIGT.

The thermal expansion coefficient of each resonating cavity is routinely determined very accurately over a wide temperature range using *in situ* microwave measurements while the cavity is evacuated,[8,9,20] and found to agree with the OFHC copper α_{L} reference data[42] (with corrected fit coefficients[46] as per Ref. 20).

The temperature-dependent constant-pressure specific heat capacity c_{p} and mass density ρ_{solid} of copper are needed for the calculation of the Grüneisen parameter γ in Eq. 9, to allow conversion between κ_{S} and κ_{T} in Eq. 8. A reference c_{p} data set[42] may be used in the form of a corrected fit equation:[46]

$$\log_{10} c_{\mathrm{p}} = \sum_{j=0}^{7} a_{c_{\mathrm{p}},j} \left(\log_{10} T_{90}\right)^{j} , \qquad (10)$$

with coefficients $a_{c_{\mathrm{p}},j}$ listed in Table I. The value of

TABLE I. Numerical values of the coefficients $a_{c_{\mathrm{p}},j}$ in Eq. 10.[46]

j	$a_{c_{\mathrm{p}},j}$
0	-1.91844
1	-0.15973
2	8.61013
3	-18.996
4	21.9661
5	-12.7328
6	3.54322
7	-0.3797

ρ_{solid} near room temperature is either taken from reference data[42] or new measurements of small material samples,[9] and then extrapolated to other temperatures using the thermal expansion measured *in situ* with microwaves.[5,7,9] But in all cases, uncertainties in ρ_{solid} and c_{p} make minimal contributions to overall RIGT uncertainties.[5,7,9] Indeed, for copper, γ is very nearly temperature independent.[33]

Finally, the combination of electrical conductivity σ_{Cu} and relative magnetic permeability $\mu_{\mathrm{r,Cu}}$ of the skin layer of the copper shell bounding the resonating cavity can also be determined *in situ* from the half-widths of the microwave resonance peaks.[8,9,20] Optimal internal consistency of RIGT results using a range of different resonance frequencies is obtained[5] when unwanted effects due to antenna overcoupling, the equatorial seam between resonator hemispheres and the anomalous skin effect are minimized via the following procedure:[5]

1. Measure microwave resonance peak half-widths of several resonant modes at low temperatures. Using only those resonance peaks with surface currents that do not cross the resonator equatorial seam, and a reference data equation for $\mu_{\mathrm{r,Cu}}(T_{90})$,[42] calculate $\sigma_{\mathrm{Cu}}(T_{90}, f)$ from the microwave measurements, where f is the microwave peak frequency.

2. Fit and extrapolate the $\sigma_{\mathrm{Cu}}(T_{90}, f)$ data to zero frequency at each temperature T_{90} to obtain $\sigma_{\mathrm{Cu},f\to 0}(T_{90})$.

3. Fit and extrapolate the $\sigma_{\mathrm{Cu},f\to 0}(T_{90})$ data to absolute zero temperature to obtain $\sigma_{\mathrm{Cu},f\to 0,T_{90}\to 0}$.

4. Analyze RIGT measurements collected with the same resonator at all temperatures and microwave frequencies using temperature-dependent, frequency-independent reference data equations for the relative magnetic permeability[42] and electrical resistivity[42] of copper. The residual resistivity free parameter in the electrical resistivity equations is calculated from $\sigma_{\mathrm{Cu},f\to 0,T_{90}\to 0}$. (Typographical errors in these reference equations must be corrected as in Ref. 20.)

3.3. Optical RIGT: optical window distortion

For optical RIGT, the most important effect of gas pressure on the experimental apparatus is distortion of the optical windows. Different methods are used to correct for this distortion in different optical RIGT technologies.

The monolithic interferometer for refractometry (MIRE) approach integrates a gas triple-cell into a quad-pass differential heterodyne interferometer. It has been used for absolute measurements of k_{B} using helium as the working gas[26] and measurements of A_{R} of multiple gases referenced to helium[17] (asterisks and diamonds in Fig. 1). By comparing measurements made using gas triple-cells that have different lengths but nominally the same optical windows, the effects of window distortion under pressure can be separated out and corrected. However, the residual uncertainty of this correction is still the single largest uncertainty component on RIGT implementations based on MIRE, contributing a relative standard uncertainty of 9.8 ppm.[17,26]

The fixed length optical cavity (FLOC) approach is based on a dual-cavity Fabry-Perot refractometer. It has been used to realize a primary pressure standard[12] and could potentially be employed for primary thermometry as well[10] (open and filled triangles in Fig. 1). This is an indirect relative RIGT technique, in which the pressure-induced distortion of the cavity is determined *in situ* using optical measurements with helium as the working gas at known p_{ref} and T_{ref}, much like the *in situ* measurements of $\kappa_{\mathrm{T,eff}}(T_{\mathrm{ref}})$ described in Sec. 3.1 for microwave RIGT. RIGT measurements are then made with nitrogen as the working gas, which is less sensitive to apparatus distortions than is helium-based RIGT.

In this way, overall FLOC uncertainties can be much lower than those of MIRE: Ref. 12 lists relative standard uncertainty contributions from the distortion corrections of 0.65 ppm for the measurement cavity and 0.2 ppm for the reference cavity; and in Ref. 10 these have been improved and combined into a single 0.1 ppm relative standard uncertainty component. However, if FLOC-based RIGT is to be used for T measurements far from the T_{ref} at which the distortion was characterized, some form of extrapolation would be needed,[10] so the extrapolation and reference data issues outlined for copper in Sec. 3.1 would also need to be resolved for the glass used to construct the FLOC apparatus.

4. Pressure, temperature and chemical impurities of the working gas

4.1. Gas pressure

Other than in the direct relative RIGT case,[8] RIGT measurements of T, A_ϵ or A_{R} must be supported by independent high-accuracy measurements of the gas pressure p. This is typically accomplished by using deadweight piston pressure balances, with the pressure balance calibration uncertainty providing a lower limit on achievable RIGT uncertainties. The uncertainty of pressure balance calibrations can be reduced, but heroic efforts are required to obtain relative standard pressure uncertainties as low as 1 ppm, such as realized during DCGT measurements of k_{B}.[47]

In Eq. 2, p refers to the pressure of the portion of working gas whose refractive index is being measured. Thus, the pressure realized by the pressure balance must be corrected for the static head effect between the reference plane of the balance and the location of refractive index measurement. The static head effect is more pronounced for heavier gases: when argon, which has a mass density ten times that of helium at the same temperatures and pressures, was used as a RIGT working gas, the uncertainty in the static head correction was the dominant component in the overall uncertainty budget.[7] However, static head corrections can be calculated more accurately when RIGT cryostats are designed to limit thermal gradients along the tubes carrying the working gas to only those tube sections that are horizontal.[8,9]

4.2. Gas temperature

Similarly, RIGT measurements of p, A_ϵ or A_{R} must be supported by independent high-accuracy measurements of the gas thermodynamic temperature T. This is accomplished by measuring T_{90} using calibrated standard platinum resistance thermometers, and then correcting for the thermodynamic inaccuracy of the ITS-90 via reference values of $(T - T_{90})$[48] to obtain T.

The reference data publication[48] that represents the best thermometry community consensus estimate of $(T - T_{90})$ is now over ten years old. The uncertainty $u(T - T_{90})/T_{90}$ is as high as 30 ppm in some temperature ranges,[48] but is much smaller (1.3 ppm) near room temperature[48] where RIGT p, A_ϵ and A_{R} measurements are realized.

However, the uncertainty of the T_{90} to T conversion was still the third largest contribution to the overall uncertainty budget of an optical RIGT FLOC pressure standard.[12] Future improvements of the FLOC technique are anticipated to reduce other optical RIGT uncertainty components to a level[10] where the uncertainty in $(T-T_{90})$ may become a main limiting factor on the accuracy of primary optical pressure realizations. This situation could be alleviated by the publication of updated $(T-T_{90})$ reference values incorporating the latest high-accuracy primary thermometry measurements from the past decade.

4.3. Gas purity

RIGT data is usually analyzed under the assumption that the chosen working gas is absolutely pure, using the values of thermophysical properties for that single gas

species (Sec. 5). The possible presence of chemical impurities causing uncorrected changes to the refractive index of the gas can be estimated in RIGT uncertainty budgets via a simple mixing rule for the first order effect on A_ϵ in Eq. 1:[5,23,49]

$$A_{\epsilon,\mathrm{mix}} = \sum_m x_m A_{\epsilon,m}, \tag{11}$$

where A_ϵ is denoted as $A_{\epsilon,\mathrm{mix}}$ for the gas mixture, and $A_{\epsilon,m}$ for the gas component m at mole fraction x_m. $A_{\epsilon,m}$ values for helium, neon and argon are listed in Table II, and those for other impurity species can be found in Ref. 49. The polarizability of helium is much lower than that of most other gases, rendering RIGT implementations based on helium particularly sensitive to impurities in the working gas.[4]

As the temperature is lowered, the vapour pressures of many gas species drop dramatically, such that they no longer contribute meaningfully to the sum in equation 11. Labs that exclusively use helium as the working gas and have a reliable supply of liquid helium can take advantage of this effect by passing the working gas through a 4 K cold trap to remove all other chemical species.[8,11]

In other cases, the working gas passes through chemical filters that are very effective at removing non-noble gas impurities.[7,9] Noble gas impurities remain problematic, particularly as gas suppliers often do not check for their presence in commercial helium, neon and argon gas products. To address this issue, samples of the working gases collected from the resonating cavity during RIGT measurements were analyzed by mass spectrometry: the resulting lower detection limits on xenon in helium and neon in argon dominated the uncertainty estimations due to gas impurities (noting the overlapping mass spectrometer peaks for $^{20}\mathrm{Ne}^+$ and $^{40}\mathrm{Ar}^{++}$), yielding RIGT uncertainty components the same size as that arising from the pressure measurement.[7]

5. Thermophysical properties of the working gas

Knowledge of thermophysical gas properties represents the third key pillar of RIGT, and is an area where the reference data has leapt forward since the publication of Ref. 4. This section provides updated guidance on the current best literature values of the virial coefficients used in the analysis of RIGT experiments.

Helium has long been the best working gas for absolute RIGT because many of its properties have been calculated very accurately from first principles: it allows RIGT to provide quantum traceability to the SI, because traceability comes from quantum chemical properties of the helium atom.[10] But advancing understanding of the virial coefficients of neon and argon, along with implementation of the hybrid data analysis technique described in Sec. 2.2, has boosted the usefulness of these alternative working gases, which are less sensitive than helium to uncertainties from the other two categories. Nitrogen has also been used as a working gas for optical RIGT pressure standard realizations near room temperature, so its properties are covered here specifically in that context.

Although the hybrid data analysis method has reduced the influence of the higher virial coefficients, this method requires time-consuming measurements at many pressures on an isotherm.[7,9] Accurate knowledge of these higher-order correction terms still underpins the much faster single-state RIGT approach, which is likely to be more practical in client-facing applications such as direct thermodynamic temperature dissemination according to the new definition of the kelvin.[1,3]

Like DCGT,[50,51] RIGT data has begun to be used to extract experimental values of the higher virial coefficients[9] (see Sec. 5.3), and this application of the technique could be expanded in the future.

In optical RIGT, the electromagnetic properties of the working gas at optical frequencies are conventionally indicated by writing the working equation in terms of refractivity virial coefficients: substituting A_R in place of $(A_\epsilon + A_\mu)$ in Eq. 3; and A_R in place of A_ϵ, B_R in place of B_ϵ, and C_R in place of C_ϵ in Eqs. 4 and 5. Combined with the improved Eqs. 2–5 of the present work, these substitutions are more accurate than those listed in Eqs. 9–11 of Ref. 4. A_R, B_R and C_R are understood to be at the frequency of the measuring laser, generally a He-Ne laser with an optical wavelength of 632.9908 nm.[10,12,13,17,26,52]

Recommended reference data for the thermophysical properties of helium, neon, argon and nitrogen gases are summarized in Table II. New or updated guidance of the present work compared to Ref. 4 is indicated by a star symbol in the first column. The most accurate values derive in some cases from *ab initio* theoretical calculations and in others from experimental measurements, but either way, knowledge becomes more speculative at higher orders, with correspondingly larger or unknown uncertainties, unknown temperature dependencies, etc. Cubic splines may be used to interpolate between values provided at discrete temperatures in literature data tables. When comparing Table II to other publications, note that some authors drop the virial coefficient subscripts, instead using $B \equiv B_\rho$, $C \equiv C_\rho$, $b \equiv B_\epsilon/A_\epsilon$, $c \equiv C_\epsilon/A_\epsilon$ and so on.

5.1. A_ϵ, A_μ, A_R

For helium, a new calculation of A_ϵ by Puchalski *et al.*[35] agrees with the previous best value,[52] but with uncertainty reduced from 0.12 ppm to 0.10 ppm. For neon and argon, the most accurate A_ϵ values remain those experimentally measured by Gaiser and Fellmuth using DCGT.[53] The careful measurements of Gaiser and Fellmuth, with relative standard uncertainties of 2.4 ppm, are unlikely to be eclipsed experimentally in the near future. The RIGT community could benefit from lower neon and argon A_ϵ uncertainties, particularly as future advancements reduce uncertainty contributions from

TABLE II. Recommended reference data sources for thermophysical gas properties of helium, neon, argon and nitrogen.

New?	Property	Gas	Best Reference	Source	Value (Standard Uncertainty)
⋆	A_ϵ	He	Puchalski *et al.* 2020[35]	calculation	$0.517\,254\,08(5)\,\mathrm{cm^3\ mol^{-1}}$
	A_ϵ	Ne	Gaiser & Fellmuth 2018[53]	experiment	$0.994\,711\,4(24)\,\mathrm{cm^3\ mol^{-1}}$
	A_ϵ	Ar	Gaiser & Fellmuth 2018[53]	experiment	$4.140\,686(10)\,\mathrm{cm^3\ mol^{-1}}$
	A_μ	He	Bruch & Weinhold 2000–2003[4,32,54–56]	calculation	$-7.921(4)\times10^{-6}\,\mathrm{cm^3\ mol^{-1}}$
⋆	A_μ	Ne	Lesiuk *et al.* 2020[40]	calculation	$-3.1713(71)\times10^{-5}\,\mathrm{cm^3\ mol^{-1}}$
	A_μ	Ar	Barter *et al.* 1960[4,57]	experiment	$-8.09(6)\times10^{-5}\,\mathrm{cm^3\ mol^{-1}}$
	A_R	He	Puchalski *et al.* 2016[52]	calculation	$0.520\,255\,77(6)\,\mathrm{cm^3\ mol^{-1}}$
	A_R	Ne	Egan *et al.* 2019[17]	experiment	$1.000\,211(16)\,\mathrm{cm^3\ mol^{-1}}$
	A_R	Ar	Egan *et al.* 2019[17]	experiment	$4.195\,685(64)\,\mathrm{cm^3\ mol^{-1}}$
	A_R	N_2	Egan *et al.* 2019[17]	experiment	$4.446\,107(68)\,\mathrm{cm^3\ mol^{-1}}$
⋆	B_ϵ	He	Garberoglio & Harvey 2020[37]	calculation	Sup. Mat.: Beps_He4.dat $10^{-3}\times$ 2nd col. ($10^{-3}\times$ half of 3rd col.)
⋆	B_ϵ	Ne	Song & Luo 2020[36]	calculation	Sup. Mat.: Table S3 2nd col. (3rd col.)
⋆	B_ϵ	Ar	Garberoglio & Harvey 2020[37]	calculation	Sup. Mat.: Beps_Ar40.dat 2nd col. (half of 3rd col.)
⋆	C_ϵ	He	Present work	experiment	$\{[0.0062(15)\times(T-273.16)]-0.777(96)\}\ \mathrm{cm^9\ mol^{-3}}$
⋆	C_ϵ	Ne	Present work	experiment	$\{[0.0057(36)\times(T-273.16)]-3.69(51)\}\ \mathrm{cm^9\ mol^{-3}}$
⋆	C_ϵ	Ar	Present work	experiment	$\{[0.167(86)\times(T-273.16)]-85.1(28)\}\ \mathrm{cm^9\ mol^{-3}}$
⋆	D_ϵ	He	Lallemand & Vidal 1977[50,58]	experiment	$-2.3(15)\,\mathrm{cm^{12}\ mol^{-4}}$ at 298 K
⋆	D_ϵ	Ne	Lallemand & Vidal 1977[50,58]	experiment	$3.5(77)\,\mathrm{cm^{12}\ mol^{-4}}$ at 298 K
⋆	D_ϵ	Ar	Lallemand & Vidal 1977[50,58]	experiment	$140(190)\,\mathrm{cm^{12}\ mol^{-4}}$ at 298 K
⋆	B_R	He	Garberoglio & Harvey 2020[37]	calculation	Sup. Mat.: BR_He4.dat $10^{-3}\times$ 3rd col. (unknown)
⋆	B_R	Ne	Garberoglio & Harvey 2020[37]	calculation	Sup. Mat.: BR_Ne20.dat & BR_Ne22.dat 3rd col. (unknown)
⋆	B_R	Ar	Garberoglio & Harvey 2020[37]	calculation	Sup. Mat.: BR_Ar40.dat 3rd col. (unknown)
⋆	B_R	N_2	Achtermann *et al.* 1991[12,59]	experiment	$0.81(20)\,\mathrm{cm^6\ mol^{-2}}$ at 302.919 K
⋆	C_R	He	Puchalski *et al.* 2016[26,52]	calculation	$-0.71(17)\,\mathrm{cm^9\ mol^{-3}}$ at 293.1529 K
⋆	C_R	Ar	Coulon *et al.* 1981[60]	experiment	$-79(10)\,\mathrm{cm^9\ mol^{-3}}$ at 298 K
⋆	C_R	N_2	Achtermann *et al.* 1991[12,59]	experiment	$-89(10)\,\mathrm{cm^9\ mol^{-3}}$ at 302.919 K
⋆	B_ρ	He	Czachorowski *et al.* 2020[39]	calculation	Sup. Inf.: S4_virial_helium-4.txt 2nd col. (3rd col.)
⋆	B_ρ	Ne	Present work	experiment	Table III (bracketed numbers in Table III)
⋆	B_ρ	Ar	Present work	experiment	Table III (bracketed numbers in Table III)
⋆	B_ρ	N_2	Dymond *et al.* 2002[12,61]	experiment	$\left\{-4.571+\left[\left(1.974\times10^{-1}\right)\times(T-300)\right]-\left[\left(5.137\times10^{-4}\right)\times(T-300)^2\right]\right\}\ (0.24)\ \mathrm{cm^3\ mol^{-1}}$
	C_ρ	He	Garberoglio *et al.* 2011[62,63]	calculation	Table 1 2nd col. (half of 3rd col.)
	C_ρ	Ne	Wiebke *et al.* 2012[64]	calculation	Eq. 9 & 3rd col. of Table II (unknown) [a]
	C_ρ	Ar	Cencek *et al.* 2013[65]	calculation	Table 3 2nd col. (half of 3rd col.)
⋆	C_ρ	N_2	Dymond *et al.* 2002[12,61]	experiment	$\{1432+[(2.923)\times(T-300)]-\left[(0.781)\times(T-300)^2\right]\}\ (100)\ \mathrm{cm^6\ mol^{-2}}$
⋆	D_ρ	He	Garberoglio & Harvey 2021[41]	calculation	Table I 8th col. (half of 9th col.)
	D_ρ	Ne	Wiebke *et al.* 2012[64]	calculation	Eq. 9 & 4th col. of Table II (unknown) [a]
	D_ρ	Ar	Jäger *et al.* 2011[66]	calculation	Sup. Mat.: Sec. 3 B_n(T) Eq. & 4th col. of Table B_4 (unknown)
⋆	E_ρ	He	Schultz & Kofke 2019[34]	calculation	Table 4 4th col. (bracketed numbers in 4th col.)
⋆	E_ρ	Ne	Hellmann as per Gaiser & Fellmuth 2019[50]	calculation	25 000 (unknown) $\mathrm{cm^{12}\ mol^{-4}}$ at 273.16 K
⋆	E_ρ	Ar	Jäger *et al.* 2011[66]	calculation	Sup. Mat.: Sec. 3 B_n(T) Eq. & 4th col. of Table B_5 (unknown)

[a] Typographical errors in Ref. 64 must be corrected as described in Ref. 4.

other categories. Recent theoretical progress has been made for neon,[40] but *ab initio* accuracy is not yet competitive with the experimental results for A_ϵ.

$A_\mu = 4\pi\chi_0/3$ is obtained from the diamagnetic susceptibility of one atom χ_0. The helium calculation of Bruch and Weinhold[54–56] remains current, as treated in Refs. 4 and 32 to include relativistic effects. This is different to how the Bruch and Weinhold results were treated non-relativistically in Ref. 52. A new, highly-accurate neon calculation by Lesiuk *et al.*[40] replaces the historical reference measurements of Barter *et al.*,[57] about which concerns had been raised in Ref. 4. The experimental results of Barter *et al.* for argon[57] remain unchallenged: accurate new calculations or measurements of the magnetic susceptibility of argon could resolve the A_μ situation for this gas, just as the work of Lesiuk *et al.*[40] has done for neon.

For helium, the A_R calculation by Puchalski *et al.*[52]

remains current, and for neon, argon and nitrogen the most accurate values are those experimentally measured by Egan *et al.*[17] using RIGT traceable to the properties of helium. Egan *et al.* also measured A_{R} for more exotic gases: xenon, carbon dioxide and nitrous oxide.[17]

5.2. B_ϵ, C_ϵ, D_ϵ, B_{R}, C_{R}

The inconsistency between the Moszynski *et al.*[67] and Rizzo *et al.*[68] calculations of helium B_ϵ described in Ref. 4 has now been decisively resolved by a new quantum statistical calculation of Garberoglio and Harvey[37] and a new semi-classical calculation of Song and Luo.[36] Both new papers also calculate B_ϵ for neon and argon,[36,37] and agree very well with one another. The calculation of Garberoglio and Harvey[37] fully includes quantum effects and has smaller standard uncertainties than the calculation of Song and Luo,[36] and so is preferred for helium and argon. The calculation of Song and Luo[36] is recommended for neon, since Garberoglio and Harvey[37] do not list uncertainties for their neon results, and the values of Song and Luo are in excellent agreement with those of Garberoglio and Harvey (well within Song and Luo's quoted uncertainties).

The poor knowledge and inconsistent handling of C_ϵ described in Ref. 4 remains to be resolved. Although the hybrid data analysis method reduces the overall uncertainty contribution due to the higher virial coefficients, in the Ref. 7 helium measurements this small residual uncertainty component was dominated by the uncertainty in C_ϵ. Furthermore, in a recent realization of a helium-based DCGT primary pressure standard, C_ϵ contributed the second-largest component to the overall uncertainty budget;[69] and it would have been by far the largest uncertainty component had the new helium B_ρ values of Song *et al.*[38] or Czachorowski *et al.*[39] been available to the authors of Ref. 69.

In order to ameliorate the C_ϵ data situation, experimental measurements of this quantity for helium, neon and argon have been collated in Figs. 6–8 and fitted to straight lines. All three figures include the measurements of Huot and Bose,[70] and the measurements of Lallemand and Vidal[58] as re-analyzed by Gaiser and Fellmuth[50] but restored from 273.16 K to the original measurement temperature of 298 K. Figure 6 additionally includes the measurements of: White and Gugan,[71] Kirouac and Bose[72] as re-analyzed by White and Gugan,[71] and Kerr and Sherman[73] as re-analyzed by White and Gugan.[71] The lone theoretical helium C_ϵ calculation of Heller and Gelbart[74] is plotted in Fig. 6, but not used in the fit since its publication does not state a numerical temperature and gives no indication of uncertainty.

The experimental data points are assumed to be uncorrelated and are weighted in the fits by the inverse squares of their uncertainties. The fitted coefficients are listed in Table II. New high-accuracy theoretical calculations, including uncertainty budgets, could greatly improve the

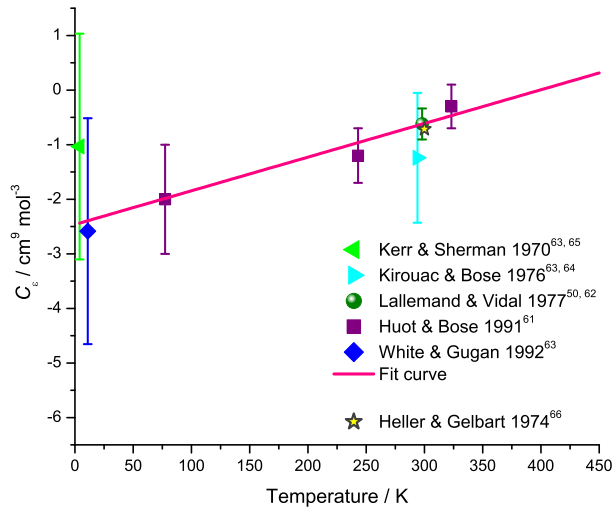

FIG. 6. C_ϵ data and fit for helium.

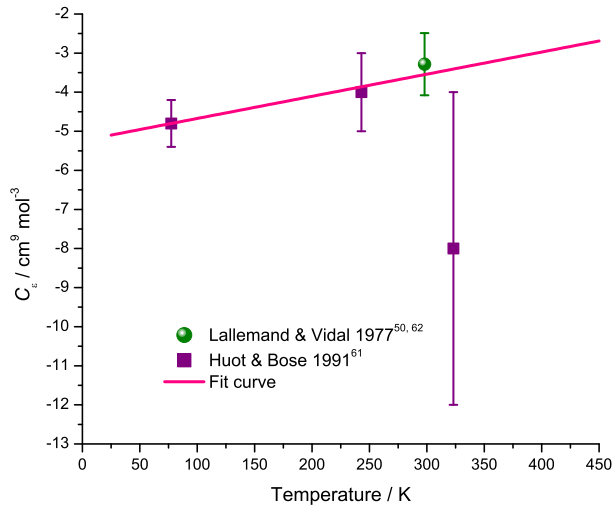

FIG. 7. C_ϵ data and fit for neon.

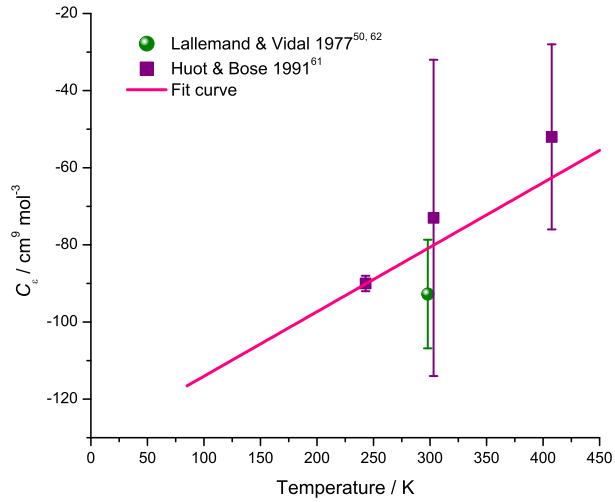

FIG. 8. C_ϵ data and fit for argon.

C_ϵ reference data for all three gases.

The measurements of Lallemand and Vidal[58] as re-analyzed by Gaiser and Fellmuth[50] give rough order-of-magnitude estimates of D_ϵ for helium, neon and argon.

Garberoglio and Harvey also calculated optical B_R values for helium, neon and argon, though without listed uncertainties.[37] The optical B_R value for nitrogen is based on the work of Achtermann *et al.*,[59] as per Ref. 12. A calculated theoretical value of the optical C_R for helium was adapted from the work of Puchalski *et al.*[52] by Egan *et al.*[26] The optical C_R value for argon comes from Coulon *et al.*,[60] and that for nitrogen is based on the work of Achtermann *et al.*,[59] as per Ref. 12. The author is not aware of calculations or measurements of C_R for neon, but Egan *et al.* suggest that their isotherm data could be reanalyzed in the future to yield new experimental values of B_R and C_R for neon, argon, nitrogen and other gases.[17]

5.3. B_ρ, C_ρ, D_ρ, E_ρ

A comparison between the latest theoretical and experimental values of B_ρ for helium, neon and argon is shown in Table III.

For helium, a new highly-accurate B_ρ calculation of Czachorowski *et al.*[39] replaces that of Cencek *et al.*,[77] reducing the uncertainty by a factor of 5 or more. A similar helium-4 calculation has been published by Song *et al.*[38] using the interatomic interaction potential that was expanded on by Czachorowski *et al.*;[39] however the helium-3 results of the two papers disagree with one another.[39]

Experimental data from the DCGT measurements of Gaiser and Fellmuth[50,51] and the RIGT measurements of Madonna Ripa *et al.*[9] are re-analyzed here to give B_ρ using the new calculated helium and argon B_ϵ values of Garberoglio and Harvey[37] and neon B_ϵ values of Song and Luo.[36] The agreement between all experiment and theory results in Table III is generally good, considering their mutual uncertainties. The theoretically-calculated B_ρ values for helium and experimentally-measured B_ρ values for neon and argon are accurate enough for single-state RIGT analysis. Away from the temperatures of the experimental measurements, the calculated B_ρ values of Wiebke *et al.*[64] for neon and Jäger *et al.*[66] for argon are recommended to be used to support hybrid RIGT analysis, but are insufficient for single-state RIGT. New high-accuracy theoretical calculations, including uncertainty budgets, could improve the B_ρ reference data for neon and argon.

To get B_ρ for nitrogen, Egan *et al.* fitted the earlier experimental data of Dymond *et al.*[61] in the temperature range from 290 K to 310 K.[12] Egan *et al.* also directly obtained a more accurate nitrogen $B_\rho = -3.973(35)\,\mathrm{cm^3\ mol^{-1}}$ at 302.919 K from their experimental optical RIGT measurements,[12] so optical RIGT applications at exactly this temperature should use this value rather than the fit to the data of Dymond *et al.*[61]

The C_ρ calculation of Garberoglio *et al.* remains current for helium, as it includes quantum effects and has a full uncertainty budget including the uncertainty contribution from the potential.[62,63] The neon calculation of Wiebke *et al.*[64] also remains current, correcting a typographical error as in Ref. 4. An estimated uncertainty in the C_ρ value of Wiebke *et al.*[64] at 273.16 K is reported by Gaiser and Fellmuth from a private communication by Hellmann of the University of Rostock, Germany.[50]

For argon, the C_ρ calculation of Cencek *et al.*[65] continues to be recommended, since it is fully quantum mechanical and has a rigorous uncertainty budget; the tabulated values are sparsely spaced, but errors introduced by interpolating between them should remain less than the uncertainties of the calculations themselves. As an alternative, the calculation represented by the fit equation in section 3 of the supplementary material of Jäger *et al.*,[66] with coefficients from the 4$^\mathrm{th}$ column of the B_3 table of the same, can be applied at any temperature and agrees with the values of Cencek *et al.* well within Cencek *et al.*'s uncertainties.[65]

C_ρ for nitrogen is a fit to the data of Dymond *et al.*[61] performed by Egan *et al.* in the temperature range from 290 K to 310 K.[12]

A new state-of-the-art helium D_ρ calculation by Garberoglio and Harvey uses the newest potentials, fully includes exchange effects, and is presented with a complete uncertainty budget including the uncertainty contribution from the potential.[41] The D_ρ neon calculation of Wiebke *et al.*[64] remains current, correcting two typographical errors as in Ref. 4. The D_ρ calculation for argon of Jäger *et al.*[66] also remains current.

A new calculation of E_ρ for helium by Schultz and Kofke covers a wide temperature range, but does not include the effects of exchange and has an incomplete uncertainty budget missing the uncertainty contribution from the potential.[34] The tabulated values may be interpolated by the fit equation 6 of Schultz and Kofke, with coefficients from the 5$^\mathrm{th}$ column of Table 7 of the same.[34] A preliminary calculation of E_ρ for neon at 273.16 K is reported by Gaiser and Fellmuth from a private communication by Hellmann.[50] An E_ρ calculation for argon in included in the publication of Jäger *et al.*[66]

6. Conclusions

The present work has reviewed the data landscape of the refractive-index gas thermometry field, focusing on the latest developments and remaining challenges since the publication of the previous review article,[4] and also including important applications outside of direct realization of the kelvin, such as primary gas pressure standards.

The three dominant categories of RIGT uncertainties arise from: pressure-induced compression and distortions

TABLE III. Second density virial coefficient B_ρ values for helium, neon and argon. All columns are in units of $\mathrm{cm}^3\ \mathrm{mol}^{-1}$.

Reference	$T = 13.804\,\mathrm{K}$	$T = 24.555\,\mathrm{K}$	$T = 54.355\,\mathrm{K}$	$T = 83.801\,\mathrm{K}$	$T = 161.399\,\mathrm{K}$	$T = 273.16\,\mathrm{K}$
Helium: theory						
Song *et al.* 2020[38] [a]	−11.844(2)	0.951 37(134)	9.2914(6)	11.2247(4)	12.1890(2)	11.9281(1)
Czachorowski *et al.* 2020[39] [a]	−11.8436(24)	0.9514(13)	9.291 23(61)	11.224 61(40)	12.188 93(22)	11.928 11(13)
Helium: experiment						
Gaiser & Fellmuth 2019/2021 DCGT[50,51]	−11.83(5)	0.96(3)	9.28(2)	11.23(3)	12.24(14)	11.9258(15)
Madonna Ripa *et al.* 2021 RIGT[9]	−11.834(33) [b]	0.918(21) [b]	9.277(17) [b]	11.253(30) [b]	12.189(78) [b]	
Neon: theory						
Bich *et al.* 2008[75] [c]			−30.812	−9.987	5.466	10.964(55) [d]
Wiebke *et al.* 2012[64] [c]			−30.740	−9.960	5.464	10.973(55) [d]
Neon: experiment						
Gaiser & Fellmuth 2019 DCGT[50]						10.9859(51)
Madonna Ripa *et al.* 2021 RIGT[9]			−30.673(42) [b]	−9.930(17) [b]	5.425(11) [b]	
Argon: theory						
Jäger *et al.* 2011[66] [e]					−74.74	−21.19(20) [d]
Wiebke *et al.* 2011[76] [e]					−73.42	−21.38(21) [d]
Mehl in Sup. B of Moldover *et al.* 2014[32]					−74.59(25)	−21.12(13)
Argon: experiment						
Gaiser & Fellmuth 2019 DCGT[50]						−21.218(15)

[a] Not independent calculations: based on similar helium potentials, though expanded upon by Czachorowski *et al.*.[39]
[b] Incomplete uncertainty budget: only statistical fitting uncertainty.
[c] Not independent calculations: based on the same neon potentials.[50]
[d] Uncertainty at 273.16 K from private communication by Hellmann, as reported by Gaiser and Fellmuth.[50]
[e] Not independent calculations: based on the same argon potentials.[50]

of the apparatus; independent measurements of the gas pressure, temperature and composition; and the thermophysical gas properties used to analyze RIGT results. These have been mitigated by recent advancements such as *in situ* measurement of pressure effects on each RIGT apparatus, direct relative single-state RIGT, hybrid data analysis, repeated measurements using different working gases, and new *ab initio* calculations. Yet limitations still remain in each uncertainty category.

The *in situ* measurement of microwave cavity compressibility at a reference temperature, and extrapolation to other temperatures of interest, has significantly reduced RIGT uncertainty budgets. However, the extrapolation relies on the assumed temperature independence of the Anderson-Grüneisen parameter δ, and internal consistency tests of the extrapolation procedure on historical reference bulk modulus data sets for copper suggest that this assumption breaks down at low temperatures, causing the extrapolated compressibility to deviate from the measured compressibility. New highly-accurate measurements of the bulk modulus of copper between 4 K and 300 K are needed to clarify the situation.

When RIGT is applied as a primary pressure standard, the temperature must be simultaneously measured using a thermometer calibrated on the International Temperature Scale of 1990 and converted to thermodynamic temperature using thermometry community consensus data for the thermodynamic inaccuracy of the scale. But the relevant reference publication is over 10 years old, and anticipated advancements in optical RIGT may lead to the accuracy of primary RIGT pressure standards becoming limited by the uncertainty in the temperature conversion. A comprehensive updated assessment of temperature scale thermodynamic inaccuracy that includes the new data collected over the past 10 years could help support the pressure metrology community.

Great progress has also been made in the knowledge of thermophysical properties of RIGT working gases, and this is reflected in the updated reference data recommendations of Table II. New state-of-the-art theoretical calculations of A_μ for neon (via the diamagnetic susceptibility χ_0) and B_ϵ for helium have resolved previously-identified inconsistencies in the literature, new calculations of B_ϵ for neon and argon have sharpened the understanding of these gases, and a new calculation of B_ρ for helium has reduced its uncertainty by a factor of 5 or more.

In the present work, experimental data from the literature have been analyzed to give improved values of C_ϵ for helium, neon and argon, and B_ρ for neon and argon. Although in these cases new highly-accurate *ab initio* calculations over a broad temperature range, with robust uncertainty estimates, are needed to support fast single-state RIGT applications. RIGT implementations that use neon or argon would also benefit from more accurate determinations of A_ϵ, and improved knowledge of A_μ for argon from new calculations or measurements of the diamagnetic susceptibility χ_0 would resolve inconsistencies in the existing literature (as has now been done for neon). Better calculations or measurements of B_R for nitrogen and C_R for helium, neon, argon and nitrogen would be welcome in optical RIGT; especially neon C_R, for which information is lacking.

ACKNOWLEDGMENTS

The author would like to thank Christof Gaiser for stimulating discussions that informed Secs. 3.1 and 5.

7. References

[1] M. Stock, R. Davis, E. de Mirandés, and M. J. T. Milton, Metrologia **56**, 022001 (2019).
[2] BIPM, SI Brochure (9th edition, v1.08, ISBN 978-92-822-2272-0) (2019), https://www.bipm.org/en/publications/si-brochure/.
[3] CCT, Mise en pratique for the definition of the kelvin in the SI (2019), https://www.bipm.org/utils/en/pdf/si-mep/SI-App2-kelvin.pdf.
[4] P. M. C. Rourke, C. Gaiser, B. Gao, D. Madonna Ripa, M. R. Moldover, L. Pitre, and R. J. Underwood, Metrologia **56**, 032001 (2019).
[5] P. M. C. Rourke, International Journal of Thermophysics **38**, 107 (2017).
[6] J. Cui, X.-J. Feng, H. Lin, J.-T. Zhang, and K.-W. Huan, Jiliang Xuebao / Acta Metrologica Sinica **39**, 255 (2018).
[7] P. M. C. Rourke, Metrologia **57**, 024001 (2020).
[8] B. Gao, H. Zhang, D. Han, C. Pan, H. Chen, Y. Song, W. Liu, J. Hu, X. Kong, F. Sparasci, M. Plimmer, E. Luo, and L. Pitre, Metrologia **57**, 065006 (2020).
[9] D. Madonna Ripa, D. Imbraguglio, C. Gaiser, P. P. M. Steur, D. Giraudi, M. Fogliati, M. Bertinetti, G. Lopardo, R. Dematteis, and R. M. Gavioso, Metrologia **58**, 025008 (2021).
[10] J. Ricker, K. O. Douglass, S. Syssoev, J. Stone, S. Avdiaj, and J. Hendricks, Metrologia (2021), (in press).
[11] J. W. Schmidt, R. M. Gavioso, E. F. May, and M. R. Moldover, Physical Review Letters **98**, 254504 (2007).
[12] P. F. Egan, J. A. Stone, J. E. Ricker, and J. H. Hendricks, Review of Scientific Instruments **87**, 053113 (2016).
[13] K. Jousten, J. Hendricks, D. Barker, K. Douglas, S. Eckel, P. Egan, J. Fedchak, J. Flügge, C. Gaiser, D. Olson, J. Ricker, T. Rubin, W. Sabuga, J. Scherschligt, R. Schödel, U. Sterr, J. Stone, and G. Strouse, Metrologia **54**, S146 (2017).
[14] D. Mari, M. Pisani, and M. Zucco, Measurement **132**, 402 (2019).
[15] Y. Takei, K. Arai, H. Yoshida, Y. Bitou, S. Telada, and T. Kobata, Measurement **151**, 107090 (2020).
[16] E. F. May, L. Pitre, J. B. Mehl, M. R. Moldover, and J. W. Schmidt, Review of Scientific Instruments **75**, 3307 (2004).
[17] P. F. Egan, J. A. Stone, J. K. Scherschligt, and A. H. Harvey, Journal of Vacuum Science & Technology A **37**, 031603 (2019).
[18] R. Underwood, D. Flack, P. Morantz, G. Sutton, P. Shore, and M. de Podesta, Metrologia **48**, 1 (2011).
[19] X. J. Feng, K. A. Gillis, M. R. Moldover, and J. B. Mehl, Metrologia **50**, 219 (2013).
[20] P. M. C. Rourke and K. D. Hill, International Journal of Thermophysics **36**, 205 (2015).
[21] M. R. Moldover, J. W. Schmidt, K. A. Gillis, J. B. Mehl, and J. D. Wright, Measurement Science and Technology **26**, 015304 (2015).
[22] K. Zhang, X. J. Feng, J. T. Zhang, H. Lin, Y. N. Duan, and Y. Y. Duan, Measurement Science and Technology **28**, 015006 (2017).
[23] R. Cuccaro, R. M. Gavioso, G. Benedetto, D. Madonna Ripa, V. Fernicola, and C. Guianvarc'h, International Journal of Thermophysics **33**, 1352 (2012).
[24] R. J. Underwood, R. Cuccaro, S. Bell, R. M. Gavioso, D. Madonna Ripa, M. Stevens, and M. de Podesta, Measurement Science and Technology **23**, 085905 (2012).
[25] R. M. Gavioso, D. Madonna Ripa, R. Benyon, J. G. Gallegos, F. Perez-Sanz, S. Corbellini, S. Avila, and A. M. Benito, International Journal of Thermophysics **35**, 748 (2014).
[26] P. F. Egan, J. A. Stone, J. E. Ricker, J. H. Hendricks, and G. F. Strouse, Optics Letters **42**, 2944 (2017).
[27] I. Silander, T. Hausmaninger, M. Zelan, and O. Axner, Journal of Vacuum Science & Technology A **36**, 03E105 (2018).
[28] I. Silander, T. Hausmaninger, C. Forssén, M. Zelan, and O. Axner, Journal of Vacuum Science & Technology B **37**, 042901 (2019).
[29] I. Silander, C. Forssén, J. Zakrisson, M. Zelan, and O. Axner, Optics Letters **45**, 2652 (2020).
[30] J. Zakrisson, I. Silander, C. Forssén, M. Zelan, and O. Axner, Journal of Vacuum Science & Technology B **38**, 054202 (2020).
[31] C. Gaiser, T. Zandt, and B. Fellmuth, Metrologia **52**, S217 (2015).
[32] M. R. Moldover, R. M. Gavioso, J. B. Mehl, L. Pitre, M. de Podesta, and J. T. Zhang, Metrologia **51**, R1 (2014).
[33] C. Gaiser and B. Fellmuth, Physica Status Solidi b **253**, 1549 (2016).
[34] A. J. Schultz and D. A. Kofke, Journal of Chemical & Engineering Data **64**, 3742 (2019).
[35] M. Puchalski, K. Szalewicz, M. Lesiuk, and B. Jeziorski, Physical Review A **101**, 022505 (2020).
[36] B. Song and Q.-Y. Luo, Metrologia **57**, 025007 (2020).
[37] G. Garberoglio and A. H. Harvey, Journal of Research of NIST **125**, 125022 (2020).
[38] B. Song, P. Xu, and M. He, Molecular Physics **119**, e1802525 (2020).
[39] P. Czachorowski, M. Przybytek, Lesiuk, Puchalski, and B. Jeziorski, Physical Review A **102**, 042810 (2020).
[40] M. Lesiuk, M. Przybytek, and B. Jeziorski, Physical Review A **102**, 052816 (2020).
[41] G. Garberoglio and A. H. Harvey, Journal of Chemical Physics **154**, 104107 (2021).
[42] N. J. Simon, E. S. Drexler, and R. P. Reed, NIST Monograph **177** (1992).
[43] E. Grüneisen, Annalen der Physik **344**, 257 (1912).
[44] W. C. Overton and J. Gaffney, Physical Review **98**, 969 (1955).
[45] H. M. Ledbetter, Physica Status Solidi a **66**, 477 (1981).
[46] Material Properties: OFHC Copper (UNS C10100/C10200), NIST Cryogenic Material Properties Database (2010), https://trc.nist.gov/cryogenics/materials/materialproperties.htm.
[47] C. Gaiser, B.Fellmuth, N. Haft, A. Kuhn, B. Thiele-Krivoi, T. Zandt, J. Fischer, O. Jusko, and W. Sabuga, Metrologia **54**, 280 (2017).
[48] J. Fischer, M. de Podesta, K. D. Hill, M. Moldover, L. Pitre, R. Rusby, P. Steur, O. Tamura, R. White, and L. Wolber, International Journal of Thermophysics **32**, 12 (2011).
[49] A. H. Harvey and E. W. Lemmon, International Journal of Thermophysics **26**, 31 (2005).
[50] C. Gaiser and B. Fellmuth, Journal of Chemical Physics **150**, 134303 (2019).
[51] C. Gaiser and B. Fellmuth, Metrologia **58**, 015013 (2021).
[52] M. Puchalski, K. Piszczatowski, J. Komasa, B. Jeziorski, and K. Szalewicz, Physical Review A **93**, 032515 (2016).
[53] C. Gaiser and B. Fellmuth, Physical Review Letters **120**, 123203 (2018).
[54] L. W. Bruch and F. Weinhold, Journal of Chemical Physics **113**, 8667 (2000).
[55] L. W. Bruch and F. Weinhold, Journal of Chemical Physics **117**, 3243 (2002).
[56] L. W. Bruch and F. Weinhold, Journal of Chemical Physics **119**, 638 (2003).
[57] C. Barter, R. G. Meisenheimer, and D. P. Stevenson, Journal of Physical Chemistry **64**, 1312 (1960).
[58] M. Lallemand and D. Vidal, Journal of Chemical Physics **66**, 4776 (1977).
[59] H. J. Achtermann, G. Magnus, and T. K. Bose, Journal of Chemical Physics **94**, 5669 (1991).
[60] R. Coulon, G. Montixi, and R. Occelli, Canadian Journal of Physics **59**, 1555 (1981).
[61] J. D. Dymond, K. N. Marsh, R. C. Wilhoit, and K. C. Wong, *Virial Coefficients of Pure Gases and Mixtures*, Landolt–Börnstein, Group IV: Physical Chemistry, Vol. 21

(Springer–Verlag, Berlin, 2002).
[62]G. Garberoglio, M. R. Moldover, and A. H. Harvey, Journal of Research of NIST **116**, 729 (2011).
[63]G. Garberoglio, M. R. Moldover, and A. H. Harvey, Journal of Research of NIST **125**, 125019 (2020).
[64]E. Bich, R. Hellmann, and E. Vogel, Journal of Chemical Physics **137**, 0114508 (2012).
[65]W. Cencek, G. Garberoglio, A. H. Harvey, M. O. McLinden, and K. Szalewicz, Journal of Physical Chemistry A **117**, 7542 (2013).
[66]B. Jäger, R. Hellmann, E. Bich, and E. Vogel, Journal of Chemical Physics **135**, 084308 (2011).
[67]R. Moszynski, T. G. A. Heijmen, and A. van der Avoird, Chemical Physics Letters **247**, 440 (1995).
[68]A. Rizzo, C. Hättig, B. Fernández, and H. Koch, Journal of Chemical Physics **117**, 2609 (2002).
[69]C. Gaiser, B. Fellmuth, and W. Sabuga, Nature Physics **16**, 177 (2020).
[70]J. Huot and T. K. Bose, Journal of Chemical Physics **95**, 2683 (1991).
[71]M. P. White and D. Gugan, Metrologia **29**, 37 (1992).
[72]S. Kirouac and T. K. Bose, Journal of Chemical Physics **64**, 1580 (1976).
[73]E. C. Kerr and R. H. Sherman, Journal of Low Temperature Physics **3**, 451 (1970).
[74]D. F. Heller and W. M. Gelbart, Chemical Physics Letters **27**, 359 (1974).
[75]E. Bich, R. Hellmann, and E. Vogel, Molecular Physics **106**, 1107 (2008).
[76]J. Wiebke, P. Schwerdtfeger, G. E. Moyano, and E. Pahl, Chemical Physics Letters **514**, 164 (2011).
[77]W. Cencek, M. Przybytek, J. Komasa, J. B. Mehl, B. Jeziorski, and K. Szalewicz, Journal of Chemical Physics **136**, 224303 (2012).